Naval Research Laboratory
Washington, DC 20375-5320

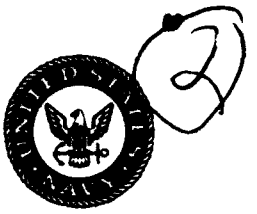

NRL/MR/6790--94-7408

Design of a High Power X-Band Magnicon Amplifier

S. H. GOLD

Beam Physics Branch
Plasma Physics Division

O. A. NEZHEVENKO
V. P. YAKOVLEV

Budker Institute of Nuclear Physics
630090, Novosibirsk, Russia

B. HAFIZI

Icarus Research
Bethesda, Maryland

February 14, 1994

REPORT DOCUMENTATION PAGE

Form Approved
OMB No. 0704-0188

1. AGENCY USE ONLY (*Leave Blank*)	2. REPORT DATE	3. REPORT TYPE AND DATES COVERED
	February 14, 1994	Interim

4. TITLE AND SUBTITLE

Design of a High Power X-Band Magnicon Amplifier

5. FUNDING NUMBERS

PE - 61153N

6. AUTHOR(S)

O. A. Nezhevenko,* V. P. Yakovlev,* S. H. Gold, and B. Hafizi**

7. PERFORMING ORGANIZATION NAME(S) AND ADDRESS(ES)

Naval Research Laboratory
Washington, DC 20375-5320

8. PERFORMING ORGANIZATION REPORT NUMBER

NRL/MR/6790--94-7408

9. SPONSORING/MONITORING AGENCY NAME(S) AND ADDRESS(ES)

Office of Naval Research
Arlington, VA 22217-5660

U.S. Department of Energy
Washington, DC 20545

10. SPONSORING/MONITORING AGENCY REPORT NUMBER

11. SUPPLEMENTARY NOTES

*Visiting Scholar, FM Technologies and George Mason University, Fairfax, VA 22021.
Permanent address: Budker Institute of Nuclear Physics, 630090, Novosibirsk, Russia.
**Icarus Research, 7113 Exfair Rd., Bethesda, MD 20814.

12a. DISTRIBUTION/AVAILABILITY STATEMENT

Approved for public release; distribution unlimited.

12b. DISTRIBUTION CODE

13. ABSTRACT (*Maximum 200 words*)

We present a design study for an X-band frequency-doubling magnicon amplifier driven by a 500 keV, 172 A beam from a field-emission diode. This study makes use of steady-state particle simulations employing the realistic fields of magnicon cavities connected by beam tunnels, and includes the effects of finite electron beam diameter. The simulations propagate an electron beam through a sequence of deflection cavities at 5.7 GHz, followed by an output cavity that operates at 11.4 GHz. The deflection cavities and the output cavity contain synchronously rotating TM modes. The deflection cavities progressively spin up the beam transverse momentum, until $\alpha \equiv v_\perp / v_z \geq 1$, where $v_\perp$ and v_z are the velocity components perpendicular and parallel to the axial magnetic field. The output cavity uses this synchronously gyrating beam to generate microwave radiation at twice the drive frequency. Self-consistency of the simulation is achieved by iteration until power balance exists in each cavity, and until the optimum rf phase in each cavity is determined. The final magnicon circuit should produce 20 to 50 MW at 11.4 GHz, depending on initial beam diameter, with a drive power of 1 kW at 5.7 GHz.

14. SUBJECT TERMS

Magnicon
X-band
Simulation
Microwave amplifier

15. NUMBER OF PAGES

46

16. PRICE CODE

17. SECURITY CLASSIFICATION OF REPORT	18. SECURITY CLASSIFICATION OF THIS PAGE	19. SECURITY CLASSIFICATION OF ABSTRACT	20. LIMITATION OF ABSTRACT
UNCLASSIFIED	UNCLASSIFIED	UNCLASSIFIED	UL

NSN 7540-01-280-5500

Standard Form 298 (Rev. 2-89)
Prescribed by ANSI Std 239-18
298-102

CONTENTS

DESIGN OF A HIGH POWER X-BAND MAGNICON AMPLIFIER

I. INTRODUCTION

The magnicon [1-3], a "scanning beam" microwave amplifier related to the gyrocon [4], is a possible replacement for klystron amplifiers in future electron linear accelerators operating at frequencies in the X-band and above. Compared to the klystron, the magnicon offers the potential of higher power operation at frequencies greater than 10 GHz, higher efficiency, and reduced sensitivity to variations in load impedance, while preserving the traditional klystron attributes of high gain and frequency and phase stability. These characteristics may also make the magnicon an attractive device at lower frequencies (0.5-10 GHz), for a variety of applications in which frequency and phase stability, combined with high overall efficiency, are important criteria. Such applications include high average power proton accelerators for tritium production and radioactive waste transmutation (see Ref. [5] and references therein), and microwave power beaming [6].

The magnicon consists of a number of TM-mode deflection cavities (a drive cavity and a series of gain cavities), followed by an output cavity. The deflection cavities spin up an electron beam to high transverse momentum, i.e., $\alpha \equiv v_\perp / v_z \geq 1$, where $v_\perp$ and v_z are the velocity components perpendicular and parallel to the axial magnetic field. They are typically designed so that the electron transit time is half an rf period. However, the final deflection cavity, also known as the penultimate cavity, may consist of several sections, coupled by irises, in order to reduce the rf fields required to spin the beam up to high α. The deflection cavities employ a rotating TM_{110} mode, producing a gyrating electron beam whose centroid rotates about the

Manuscript approved November 16, 1993.

cavity axis at the drive frequency. In addition, the sense of all electron velocities and displacements change in synchronism with the advance in phase of the rf wave. The output cavity extracts principally the transverse electron momentum in a gyroresonant "fast-wave" interaction that extends over several wavelengths. It employs a mode that rotates synchronously with the beam centroid motion, making possible a highly efficient output interaction without requiring beam bunching.

In order to extrapolate magnicon operation to high frequencies (>5 GHz), it is possible to operate the output cavity at a multiple of the frequency of the deflection cavities [2, 7, 8]. In this case, the output cavity will employ a TM_{m10} mode, where m is an integer greater than 1. This permits larger cavities, and lower rf fields, in the deflection system than would be required if the entire device operated at the output frequency. However, the penalty is a likely lowering of the efficiency, due to the weaker rf fields near the axis of the output cavity for $m>1$. The most practical value of m for a frequency multiplying magnicon is $m=2$. In this case, the output cavity operates in the TM_{210} mode at twice the drive frequency. An added advantage of the frequency-doubling configuration is that approximately the same magnetic field can be employed in the deflection cavities and in the output cavity. This is because the optimum magnetic field in the deflection cavities corresponds to a gyrofrequency approximately *twice* the operating frequency of the deflection cavities [1], while in the output cavity it corresponds to a gyrofrequency approximately equal to the operating frequency [2]. A generic frequency doubling magnicon configuration is illustrated in Fig. 1.

This paper presents the results of a design study to produce a circuit for an 11.4 GHz frequency-doubling magnicon amplifier experiment on the NRL Long-Pulse Accelerator (LPA) Facility [9]. The study assumes that the experiment will make

use of certain existing laboratory equipment. This includes a single-shot Marx generator power supply driving an explosive emission diode to produce a ~500 keV, 172 A, 5.5-mm-diameter solid electron beam [10]. The effect of finite beam diameter was a particular concern in this study. In addition, the study assumes that the magnetic field will be produced by a set of existing pancake magnets. These magnets are 3-cm thick, with a coil inner and outer radius of 7.9 cm and 15.75 cm. They are typically separated by 3.3-cm spacers. However, the spacing may be varied to tailor the magnetic field profile. Alternatively, the magnet may be separated into several sections, which may be powered by separate power supplies.

II. THEORETICAL MODELING AND DESIGN PROCEDURE

A. Physical Model

This study makes use of steady-state particle simulation employing the realistic fields of magnicon cavities connected by beam tunnels, and includes the effects of finite electron beam diameter. However, it does not model either space charge or beam emittance. Following the analytical determination of approximate cavity dimensions and operating parameters, the simulation procedure begins by solving for the eigenmodes of particular cavity configurations, including the effects of beam tunnels. A particle-pusher code then integrates the trajectories of electrons through these fields, first of individual cavities, and then of an entire magnicon device. The particle code uses a steady-state model that makes use of the phase synchronism between the beam and the wave. Thus, the entire simulation is carried out by following a single temporal slice of electrons, one macroparticle deep in z.

The modeling of the magnicon must take into account the modifications to the ideal cavity rf modes caused by the presence of their connecting beam tunnels. These

"non-ideal" effects can strongly influence magnicon operation, and their evaluation requires the use of accurate rf-field solutions. Figure 2 shows rf electric field lines in the gain, penultimate, and output cavities of the magnicon circuit. One effect is a change to the effective interaction length of each cavity and to the rf–field-free regions separating the cavities. However, this can be compensated for in the design of the magnicon cavities. A more significant effect is the introduction of strong transverse fields and radial gradients in the vicinity of the cavity beam tunnel and irises. These fields and gradients, combined with a finite electron beam radius, will produce velocity spreads that reduce the coherence of the electron motion. These effects are particularly important in the penultimate and output cavities, where the combination of initial beam diameter and high induced transverse momentum requires the largest beam tunnels.

Accurate rf fields are also required to model the π-mode of the penultimate cavity, and to model field leakage between the penultimate and output cavities. In order to account for this last effect, the penultimate and output cavities are considered as a single rf structure, which is solved separately for the dipole operating mode of the penultimate cavity and the quadrupole operating mode of the output cavity (see Fig. 2b,c). These separate solutions are then superposed in the particle simulation.

B. Design Goal

The objective of this study was to design a magnicon circuit with maximum efficiency for the parameters of the proposed NRL experiment. In addition, the circuit should provide for high gain (requiring no more than ~1 kW of drive power) and for an effective Q no higher than ~1000, to provide a reasonable frequency bandwidth for the device. Finally, the circuit should be stable against oscillation.

C. Description of computer models

The magnicon codes are designed to calculate realistic rf fields in the cavities and to determine the beam electron trajectories in those fields.

Calculation of the fields for dipole or quadrupole modes of axisymmetric cavities with arbitrary shapes is performed in two stages. First, two components of the rf field are calculated using the MULTIMODE code [11]. In this code, the eigenvalue problem is solved using the r and z components of the magnetic field, H_r and H_z. In this case, there are no nonphysical solutions. Then the last component, H_ϕ, is determined from the equation

$$(\nabla^2 \vec{H})_\phi + (\omega/c)^2 H_\phi = 0 , \qquad (1)$$

where ω is the eigenfrequency and c is the speed of light. The term $(\nabla^2 \vec{H})_\phi$ contains the known component H_r. This procedure does not decrease the precision of H_ϕ. In the MULTIMODE code, eight-node second-order isoparametric finite elements are used.

Next, it is necessary to determine the components of the electric field. It is possible to do this numerically by evaluating the derivatives of the components of the magnetic field or by solving Maxwell's equations using a finite element method. However, both of these methods give unacceptably large errors. Instead, we use a boundary integral method [12]. Using the MULTIMODE code, we determine the cavity surface current density distribution:

$$\vec{j} = \vec{n} \times \vec{H} \qquad (2)$$

where $\vec{n}$ is the unit vector normal to the surface. Using the current density distribution, we can find the vector potential at any point $\vec{r}$ inside the cavity:

$$\vec{A}(\vec{r}) = \frac{\mu_0}{4\pi} \int \frac{\vec{j}(\vec{r}')}{|\vec{r} - \vec{r}'|} \exp(ik|\vec{r} - \vec{r}'|) dS' , \tag{3}$$

where $k = \omega/c$, μ_0 is the permeability of free space, $\vec{r}'$ is the surface source coordinate, dS' denotes the element on the surface, and the integral is over the entire cavity surface. Then, it is possible to find the magnetic field:

$$\vec{H} = \mu_0^{-1} \nabla \times \vec{A} . \tag{4}$$

Since only the kernel of Eq. (3) depends on $\vec{r}$, it is possible to find $\vec{H}$ by analytical differentiation of this kernel. The electric field is also determined from Maxwell's equations by analytical differentiation:

$$\vec{E} = \frac{c}{i\omega\varepsilon_0} \nabla \times \nabla \times \vec{A} \tag{5}$$

Here, ε_0 is the permittivity of free space. In this case, all six field components will satisfy Maxwell's equations, and have the same precision of calculation. For the approximation of the surface current density, we use a third-order spline fit. To increase the speed of the field calculation near the cavity axis, we use a second-order paraxial expansion for all rf field components.

The equations of motion for the beam electrons are integrated using the third-order Runga-Kutta method. During the integration, energy losses and cavity detunings are also calculated. A finite diameter electron beam is broken up into a number of macroparticles, spread uniformly over the beam cross section. Thirty-seven macroparticles are typically employed, but up to 177 macroparticles have been used to verify the accuracy of the final simulations. The beam may be modeled either with zero initial pitch angle (to model a magnetic-field-immersed diode) or zero canonical angular momentum (to model a shielded diode).

D. Design Procedure

The solution for the realistic cavity rf fields is an input to the particle simulation code, which assumes a particular amplitude and phase of the fields in each cavity, and integrates the full Lorentz equations for the electrons through these fields. Iteration is used to find self-consistent values of amplitude and phase. The correct rf phase in a particular cavity is assumed to be the phase that extracts the maximum energy from the electrons. For the gain and penultimate cavities, the rf amplitude is determined by power balance, including the effect of a finite Q due to wall losses. For the output cavity, a different procedure is followed. First, an rf field amplitude is assumed. Next, the rf phase is adjusted to optimize the efficiency for the chosen amplitude. Finally, the output Q that will yield overall power balance is calculated.

The process begins with solutions for only the penultimate and output cavities. These preliminary solutions look for an efficient interaction in the output cavity as a function of the amplitude and phase of the rf fields of both the output and penultimate cavities. The beam entering the penultimate cavity is assumed to be unperturbed by the previous cavities. Separately, the gain of the deflection cavities is optimized as a

function of their length and spacing. Interesting cases are then made self-consistent by proceeding backward from the penultimate cavity toward the drive cavity, one cavity at a time, to determine the field amplitude in each preceding cavity that will drive the beam in order to produce power balance at the fields required in the next cavity. Finally, to ensure self-consistency and overall power balance through the entire device, the cavities are solved again, sequentially, beginning with a particular signal in the drive cavity.

A separate area of concern is stability against self-excitation (oscillation). The principal area of concern is the penultimate cavity. The magnicon simulation code can be used to study the stability properties of magnicon cavities for rotating modes. This is done by looking at energy balance in a cavity for an initially unperturbed electron beam and a "small" cavity rf field. If the beam loses more energy to the cavity mode than the mode dissipates in wall losses, the mode is unstable and will grow from noise. The same energy balance calculation, using higher cavity rf fields, can determine whether the oscillation will reach large amplitude, or whether there are unstable states of "hard excitation," that might be excited during the rise of the voltage pulse. However, the magnicon simulation code can only model synchronously rotating modes, and thus cannot examine the TM_{010} (klystron) mode, which occurs at approximately 3.6 GHz in the deflection cavities. Symmetric (m=0) modes, such as the TM_{010} mode, must be evaluated by another means.

In order to estimate the penultimate cavity's klystron-mode instability threshold, it is modeled as two coupled cavities. The problem of excitation of cavities coupled by small holes has been treated by Bethe [13]. If ω_1 and ω_2 represent eigenfrequencies of the individual cavities of the penultimate cavity, the eigenfrequencies of the zero and π modes of the combined system are given by ω and

$\omega(1+\kappa)$, where κ is the coupling coefficient and $\omega \approx \omega_1 \approx \omega_2$. If $\kappa << |\omega_1 - \omega_2|/\omega$, the cavities are considered to be weakly coupled. In this limit, the frequencies of the two coupled-cavity modes will be approximately equal to the frequencies of the two uncoupled cavities. In this case, each mode will have one filled cavity and one almost empty cavity, and the cavities will oscillate independently. In this small κ limit, the threshold for oscillation may be estimated by assuming that instability can occur only if the cavity detuning caused by the beam is of the same order as the difference in the cavity eigenfrequencies.

TM_{010}–mode fluctuations in the first cavity will modulate the beam momentum, resulting in current density modulation in both of the cavities. This modulation causes both frequency detuning and a change in the beam energy. Specifically, there will be electron acceleration in the first cavity (i.e., cavity loading) and deceleration in the second cavity (cavity excitation). The relative detuning $\Delta\omega/\omega$ caused by the beam may be estimated (see the Appendix) as:

$$\Delta\omega/\omega \approx R/Q \cdot \mathrm{Im}(Y),$$

where R is the cavity shunt impedance, Q is the quality factor, and $\mathrm{Im}(Y)$ is the susceptance of the beam. The detuning for the first cavity should be smaller than for the second, since the beam is not yet modulated. To estimate the instability threshold, we will make the "worst case" assumption, that the detuning of both cavities will be of the same order and of opposite sign. The magnitude of $\mathrm{Im}(Y)$ cannot exceed the modulus of the total beam admittance, $|Y|$. It is easy to show (see the Appendix) that for a relativistic beam, $|Y| \approx I_0(\omega L/c)/(\beta^3\gamma^3 U_0)$. Here, L is the length of each cavity, I_0 is the beam current, $U_0 = m_0c^2/|e|$, where m_0 is the rest mass and e is

the charge of an electron, γ is the relativistic factor, βc is the electron velocity, and $\omega/2\pi \approx 3.6$ GHz is the rf frequency of the TM_{01} mode. Then, the threshold current may be estimated as:

$$I_0 \geq \frac{\frac{|\omega_2 - \omega_1|}{\omega}\beta^2\gamma^3 U_0}{\frac{R}{Q}\frac{\omega}{c}L} \quad . \tag{6}$$

The study reported in this paper makes use only of steady-state, or time-independent modeling. Some time-dependent issues of magnicon modeling have been explored elsewhere [14].

III. Discussion of the Final Circuit

The final magnicon circuit includes a drive cavity, two half-wavelength gain cavities, and a two-section π-mode penultimate cavity, all operating at 5.7 GHz, and finally an output cavity operating at 11.4 GHz. This configuration is illustrated schematically in Fig. 3. Figure 4 shows the same cavities to scale, drawn as an overlapping sequence of the discrete rf structures depicted in Fig. 2. Figure 4 also shows the position of the 12 pancake magnets. These are arranged in two sections, each containing 6 magnets separated by 3.3-cm spacers. The two sections are separated by a larger 6.6-cm spacer. The upper part of Fig. 4 shows the resulting magnetic field profile. The design parameters are summarized in Table I.

Figure 5 illustrates the "ideal" operation of the magnicon by analyzing the case of a single, initially on-axis electron. Notice that the electron transverse momentum, plotted as the "pitch angle" or $\tan^{-1}\alpha$, progressively increases through the deflection cavities, but that most of the increase occurs in the penultimate cavity.

Finally, the transverse momentum is reduced to near zero in the output cavity and at the same time the electron energy decreases by ~58%. (For a single electron, substantially higher efficiencies are possible if α is allowed to be >>1.)

Particular areas of the circuit are discussed in separate sections below.

A. The Drive and Gain Cavities

The spin up of the electron beam takes place in a series of deflection cavities that progressively amplify the rf signal injected into the drive cavity (see Figs. 5 and 6). The drive and gain cavities are simple cylindrical cavities utilizing a rotating TM_{110} mode. The calculated ohmic Q of these cavities is ~15000. The drive cavity will be loaded by external coupling pins, in order to match the drive signal into the beam-loaded cavity, while the gain cavities are loaded principally by the beam. The use of beam loading to lower the effective Q is discussed in Section IVB. The optimum cavity length corresponds to an electron transit time of half an rf period (π radians). The diameter of the drift tubes is 1 cm in this region of the magnicon circuit. The magnetic field was chosen to be 1.6 times the cyclotron resonant value at 500 keV. The simulation calculates that the beam will shift the cold-cavity resonant frequency by −15 MHz, and lower the Q to ~1000. The calculated transverse electric and magnetic fields along the axis of the second gain cavity are shown in Fig. 7. The transverse electric fields are the result of the beam tunnels at either end of the cavity.

B. The Penultimate Cavity

The increase of rf fields is approximately exponential in the cavities of the deflection system (see Fig. 6). As a result, the highest fields, and most of the beam spin-up, will occur in the last of these cavities, the penultimate cavity. If this cavity is

similar in design to the other deflection cavities, very high rf fields are required to reach a beam $\alpha \sim 1$. This increases the likelihood of microwave breakdown, and also can lead to significant wall losses, which will lower the overall electronic efficiency of the magnicon.

In order to lower the required fields, it is desirable to have an interaction that can be sustained in a favorable rf phase for more than half of an rf period. In particular, the use of a multisection cavity, in which the fields change by π after each half-rf-period, will serve this purpose [2, 7]. In principle, a two-section cavity should need only half of the peak rf fields, reducing the likelihood of breakdown. Furthermore, since wall heating is proportional to the square of the rf fields, such a two-section cavity would dissipate approximately half as much rf power as a single-section cavity.

A further advantage in reducing the rf fields and the wall losses would be gained by using more than two sections. However, a stability constraint militates against this. Studies have shown that three-section cavities become unstable to oscillation in the TM_{010} $\pi/2$ mode, in which the three cavities act approximately as a buncher, drift space, and catcher, in a manner analogous to a klystron [8]. Additional sections would only make matters worse.

Even a two-section cavity is significantly more likely to be unstable than a single-section cavity. The stability of the penultimate cavity against oscillation in the TM_{110} π-mode requires a lower magnetic field than the optimum field in either the half-wavelength gain cavities or the output cavity. In order to stabilize the penultimate cavity, the magnet was divided into two sections separated by 6.6 cm. The penultimate cavity is located in the vicinity of the magnetic field minimum produced by this separation (see Fig. 4).

The stability of the penultimate cavity against oscillation in the TM_{010} mode is estimated using Eq. (6). The SUPERLANS code [15] is used to calculate the properties of the TM_{01} modes of the penultimate cavity. For our case, the calculated value of R/Q is 70 Ω. Also, $\omega_1/2\pi = 3626$ MHz and $\omega_2/2\pi = 3705$ MHz. In addition, $\kappa \approx 0.25|\omega_1-\omega_2|/\omega$, implying weak coupling as discussed in Section IID. Thus, by Eq. (6), the threshold current is $I_0 \sim 440$ A, more than twice the design value of the current. One should note that a similar penultimate cavity has been used for the 7 GHz magnicon [7,8] at the Budker Institute of Nuclear Physics (INP), where the beam current is 240 A and the estimated threshold current is 400 A. In this device, the klystron-type instability has not been observed [8].

The two sections of the penultimate cavity are of equal length in the final circuit. (Cavities with unequal lengths were also evaluated.) The cavity is designed so that each of the sections will yield approximately the same absolute value for the integral of the transverse magnetic field along the cavity axis, i.e., a "balanced" cavity. This is accomplished by employing a slight difference (~0.5%) in the cavity inner radius of the two sections, to correct for the asymmetry in the beam tunnel diameters at either end of the cavity. The transverse electric and magnetic fields of the penultimate cavity mode as a function of position along the axis is shown in Fig. 8. The simulations predict a maximum rf electric field of 250 kV/cm on the walls of the penultimate cavity. They also predict that the beam will detune the cold cavity resonance by −10 MHz.

C. The Output Cavity

The output cavity of a frequency-doubling magnicon employs a quadrupole TM_{210} mode, which rotates synchronously with the TM_{110} mode of the deflection

system. The cavity length is chosen as a compromise between the high fields needed for an efficient interaction in short cavities, and the lower efficiency that results from velocity spreads (and other effects) in longer cavities. The design calls for a length of 5 cm. This corresponds to approximately 4 cyclotron periods of the electrons, assuming an initial $\alpha \sim 1$ and $\Omega_c/\omega \sim 0.8$, where Ω_c is the relativistic cyclotron frequency and ω is the angular frequency of the radiation. The maximum rf electric fields are ~250 kV/cm.

Because of the scanning beam synchronism upon which the magnicon is based, the electron-wave interaction is invariant through an rf period. Thus, for an ideal beam, perfect phase synchronism is obtained without the requirement for any bunching mechanism. However, despite the invariance in time, there is no guarantee that all the electrons emitted at a particular time will remain well bunched in position and phase as they traverse the magnicon circuit, in order to produce an efficient interaction in the output cavity. The latter requirement is ultimately a constraint on the initial beam quality and on the spatial gradients of the cavity rf fields over the cross section of the electron beam. In addition, space charge may degrade the efficiency.

Figures 9 and 10 show optimized simulations of the final magnicon circuit for a 5.5-mm-diameter "magnetized" and a 2-mm-diameter "shielded" beam. In Fig. 9, the interaction of a 5.5-mm-diameter beam with the cavity fields results in a large spread in the electron trajectories. A significant energy spread is first seen in the second gain cavity. However, the most significant phase mixing occurs in the penultimate cavity, where the electrons develop a large spread in energy and in pitch angle. The nonideal effects in both of these cavities result in large part from the large radial electric fields shown in Figs. 7 and 8. As a result, the interaction in the output cavity is relatively incoherent, and the final efficiency is only 24%, much less than 58% seen in a

comparable single particle simulation (see Fig. 5). In Fig. 10, for the 2-mm-diameter shielded beam, the entire interaction is much more coherent, resembling the single-particle simulation of Fig. 5. As a result, the final efficiency is 56%.

The 2-mm-diameter beam corresponds to the approximate parameters of the INP magnicon gun [2, 16]. The correct modeling of the interaction of a near-Brillouin beam such as that produced by the INP gun cannot be carried out without including space charge, a capability that does not presently exist. The best model to use in the absence of space charge is not clear. However, a comparable simulation for a 2-mm-diameter magnetized beam yields only a slightly lower 52% efficiency.

Complete simulations were also carried out for a 1.2-mm-diameter shielded beam and a 4-mm-diameter magnetized beam. Figure 11 plots the efficiency as a function of beam diameter for all these simulations. It is noteworthy that the efficiency falls by only a few percent up to beam diameters of 2 mm, but decreases rapidly for larger diameters. Figure 12 shows the efficiency of the output cavity as a function of the rf fields in the penultimate cavity for the case of a 5.5-mm-diameter beam. The magnicon efficiency is apparently insensitive to small variations of the penultimate cavity fields.

IV. Technical Problems and Design Features

A. Rf Fields and Breakdown

The axial electric field of the TM_{110} mode, in combination with the strong axial magnetic field required for the electron-wave interaction, creates conditions favorable for multipactor breakdown in the deflection cavities. However, this problem is no different in principle from that of many other devices, such as klystrons. Nevertheless, it may be an area of concern for single-shot, short-pulse experiments employing

relatively poor (10^{-5} Torr) vacuum pressures. Effects attributed to multipactor were observed in a preliminary experiment that measured the gain between two deflection cavities [10]. A second area of concern is true high-field microwave breakdown (field emission). In order to avoid breakdown, the peak field levels in both the penultimate cavity and the output cavity are well below the Kilpatrick limit [17].

B. Beam Loading (Gyrotropic Effect)

The interaction between the (initially axicentered) electron beam and the TM_{110} mode of the deflection cavities is highly sensitive to the value of the axial magnetic field, which determines the sign and amplitude of the energy exchange between the electrons and the mode. In addition, the sense of the axial magnetic field breaks the symmetry of the interaction, resulting in different behavior for the two orthogonal circular polarizations [1,2,18]. The "preferred" circular polarization, which produces high efficiency, co-rotates with the sense of the electron gyration.

The beam loading of the drive cavity, for the preferred circular polarization, is identically zero for an on-axis electron with no initial transverse momentum when the relativistic electron cyclotron frequency in the axial magnetic field is twice the operating rf frequency. In this case, the electron trajectory remains in the E_z=0 plane of the rotating rf mode. The loading is also near zero for a finite electron beam. As a result, the electrons can be deflected in the first cavity without gaining or losing energy. However, the beam loading of the drive and gain cavities progressively increases as the magnetic field is lowered from this value. This provides a valuable means of controlling the effective cavity Q without requiring the use of external coupling or lossy materials. Another effect of beam loading is to alter the resonant frequency of the cavities, as the reactive part of the beam-circuit interaction down-

(up-) shifts the resonance from the vacuum value for the preferred (opposite) polarization [1,10]. This shift must be accounted for in the cavity design.

C. Energy Extraction

The Q-factor of the output cavity is determined principally by the output coupling. The output coupling is chosen to yield the desired electric fields, in power balance with the beam, to achieve the optimum efficiency. In the case of the 5.5-mm-diameter beam, this requires a Q of ~800, while for the 2-mm-diameter beam, Q should be ~300. In comparison, the calculated ohmic Q of a copper output cavity is ~20,000. The output coupling may be achieved in several different geometries. The principal variants are side coupling and end coupling.

Side coupling is the method conventionally used in klystrons. Its advantages are: 1) the rf is separated from the beam, simplifying collector design, and 2) the power may be extracted directly to in-band rectangular waveguide, making it immediately available for applications. There must be at least two side couplers, separated by either 45° or 135° degrees, to provide equal loading to the two orthogonal linearly polarized components of the circularly polarized TM_{210} mode. The principal disadvantage of side coupling is the potential to break the symmetry of the quadrupole mode, causing conversion to other modes. Mode conversion into dipole modes will lead to undesirable leakage of microwave power into the penultimate cavity. To minimize this, additional wall perturbations are needed, at 90° intervals from each of the couplers, to preserve quadrupole symmetry.

The alternative is to use end coupling. For end coupling, the downstream end-wall of the output cavity will contain an iris, followed by a circular output waveguide, rather than a cut-off beam tunnel. This preserves the quadrupole symmetry. The iris

diameter and thickness are chosen to achieve the desired cavity Q-value. However, the microwave mode must pass through the collector before reaching the output window, and will also need further processing to produce a useful mode, e.g., for coupling to an accelerating structure. This is the same situation faced by most gyrotron devices, including gyroklystrons [19], although for those devices TE rather than TM modes are involved. The use of end coupling is envisioned for the first test of the magnicon circuit.

V. SUMMARY

Using a magnicon simulation code, we have designed a microwave circuit for a high power frequency-doubling magnicon amplifier at 11.4 GHz. The design study was carried out using the approximate parameters (500 keV, 172 A, 5.5-mm-diameter) of an electron beam produced from a field-emission diode on the NRL LPA Facility. Using these parameters, the predicted magnicon efficiency is 24%. Based on a large number of simulations, this design appears to be insensitive to minor variations of the various experimental parameters. However, the final efficiency depends strongly on the properties of the electron beam, with a large premium to be gained from reducing the initial beam diameter. The same circuit, if driven by a beam produced by the INP magnicon gun, should produce an efficiency exceeding 50%. The initial experiment will use the existing single-shot LPA beam. However, further development of the magnicon as a practical source in this frequency range will require the use of a rep-rated modulator combined with a high quality electron beam produced by a thermionic diode.

ACKNOWLEDGMENTS

This work was supported by the U.S. Department of Energy under Interagency Agreement No. DE-AI05-91ER40638. It was also supported in part by the Office of Naval Research. We acknowledge useful discussions with A.W. Fliflet and W.M. Manheimer.

APPENDIX

The purpose of this appendix is to outline the derivation of the expression for the relativistic beam admittance employed in Section II. The admittance represents the beam loading on the rf circuit. This derivation follows along the lines indicated in [20]. To determine the several contributions to the admittance, we shall first obtain the current modulation in the second part of the penultimate cavity (hereafter referred to as the second cavity) resulting from the velocity modulation in the first part of the penultimate cavity (hereafter referred to as the first cavity). For simplicity, the motion is assumed to be one-dimensional, and the cavities are represented by short gaps, of length d, the centers of which are separated by a distance L.

The relativistic equation of motion is

$$\frac{d}{dt}(\gamma m_0 v) = |e|\frac{\partial}{\partial z}V \tag{A1}$$

where γ is the relativistic mass factor, m_0 is the electron rest mass, v is the electron velocity along the z axis, and V is the potential difference across the first cavity. From the definition of $\gamma = (1 - v^2/c^2)^{-1/2}$, it follows that

$$\frac{d}{dt}(\gamma) = \frac{|e|v}{m_0 c^2}\frac{\partial}{\partial z}V \tag{A2}$$

Combining Eqs. (A1) and (A2), one obtains

$$\frac{d}{dt}(v) = \frac{|e|}{\gamma^3 m_0}\frac{\partial}{\partial z}V \tag{A3}$$

For the gap in the first cavity,

$$\frac{\partial}{\partial z}V = \frac{V_1}{d}\sin\omega t \ , \qquad \text{(A4)}$$

where V_1 is the peak voltage across the gap. Making use of Eqs. (A3) and (A4), and following along the lines indicated in [20], the ac current induced in the second cavity is given, in phasor notation, by:

$$I_2 = -\frac{|e|I_0V_1}{m_0\gamma^3v^2}\frac{\omega L}{v}M^2\exp\left(-j\omega L/v\right) \ ,$$

where

$$M = \frac{\sin\left(\omega d/2v\right)}{\left(\omega d/2v\right)}$$

is the beam-coupling coefficient. In phasor notation, the voltage across the first gap is $-jV_1$, and hence the electronic admittance is given by $Y_{12} \equiv -I_2/(-jV_1)$, i.e.,

$$Y_{12} = j\frac{I_0(\omega L/c)}{\left(m_0c^2/|e|\right)\gamma^3\beta^3}M^2\exp\left(-j\omega L/v\right) \ ,$$

where $\beta=v/c$. In our case, $\omega L/v \sim \pi$.

Following a similar procedure, the small-signal admittance, Y_1, of an unmodulated beam traversing the distance d across the gap in the first cavity is readily determined. The result may be expressed in the form

$$\mathrm{Re}(Y_1) = g_0 \frac{2[1-\cos(\omega d/v)] - (\omega d/v)\sin(\omega d/v)}{2(\omega d/v)^2},$$

$$\mathrm{Im}(Y_1) = g_0 \frac{2\sin(\omega d/v) - (\omega d/v)[1+\cos(\omega d/v)]}{2(\omega d/v)^2},$$

where

$$g_0 = \frac{2I_0}{(m_0 c^2/|e|)\gamma^3\beta^2}.$$

Note that for $M \approx 1$, $|Y_{12}|$ and $|Y_1|$ are of the same order of magnitude.

The total beam admittance, Y, may be written in the form

$$Y = G + j\left(\omega C - \frac{1}{\omega L}\right),$$

in terms of the lumped parameters of the equivalent parallel RLC circuit, with $G=R^{-1}$. The beam loading imparts a frequency detuning $\Delta\omega$ to the circuit with respect to the resonant frequency, $\omega = (LC)^{-1/2}$, given by

$$\frac{\Delta\omega}{\omega} = \frac{1}{2}\frac{R}{Q}\mathrm{Im}(Y),$$

where Q is the cold cavity quality factor. Since the two parts of the penultimate cavity are assumed to impart detunings of the same order of magnitude, but of opposite signs, the net detuning is given by the expression indicated in Section II.

To assess the effect of space charge on the electron bunching due to a beam of finite radius, we solve the one-dimensional relativistic Vlasov equation for the electron distribution f:

$$\frac{\partial f}{\partial t}+v\frac{\partial f}{\partial z}-|e|E\frac{\partial f}{\partial p}=0 \qquad \text{(A5)}$$

where $p=\gamma m_0 v$ is the axial momentum and E is the axial electric field. Expanding about the equilibrium distribution, Eq. (A5) relates the perturbed current, I, to the electric field. In the limit in which the wavelength is large compared to b/γ, where b is the cavity radius, we can also relate the electric field in the cavity to the current via:

$$E=-\frac{Z_0}{2\pi\beta\gamma^2}\frac{dI}{dz}\left[\ln(b/r_b)+\tfrac{1}{2}\right] ,$$

where r_b is the electron beam radius and $Z_0=(\mu_0/\varepsilon_0)^{1/2}$ is the impedance of free space. Assuming that the perturbation varies as $\exp(j\omega t-jkz)$, the effect of space-charge waves on the beam is represented by the wavenumber

$$k_p=\frac{\omega}{c}\left[\frac{I_0 Z_0}{U_0(\beta\gamma)^5}\frac{\ln(b/r_b)+\frac{1}{2}}{2\pi}\right]^{1/2} ,$$

where $U_0=m_0c^2/|e|$. For the 5.5-mm-diameter beam and cavity radius b=3.2 cm, k_p≈0.06 ω/c, indicating that space charge has a minor effect on the bunching.

REFERENCES

[1] M. Karliner, E.V. Kozyrev, I.G. Makarov, O.A. Nezhevenko, G.N. Ostreiko, B.Z. Persov, and G.V. Serdobintsev, "The Magnicon—An Advanced Version of the Gyrocon," *Nucl. Instrum. Methods Phys. Res.*, vol. A269, pp. 459-473, 1988.

[2] O.A. Nezhevenko, "The Magnicon: A New RF Power Source for Accelerators," in *Conference Record—1991 IEEE Particle Accelerator Conference*, edited by L. Lizama and J. Chew [IEEE, New York, 1991], vol. 5, p. 2933-2942.

[3] W.M. Manheimer, "Theory and Conceptual Design of a High-Power Highly Efficient Magnicon at 10 and 20 GHz," *IEEE Trans. Plasma Sci.*, vol. 18, pp. 632-645, 1990.

[4] G.I. Budker, M.M. Karliner, I.G. Makarov, S.N. Morosov, O.A. Nezhevenko, G.N. Ostreiko, and I.A. Shekhtman, "The Gyrocon—An Efficient Relativistic High-Power VHF Generator," *Part. Accel.*, vol. 10, pp. 41-59, 1979.

[5] G.P. Lawrence, "High Power Proton Linac for Transmuting the Long-Lived Fission Products of Nuclear Waste," in *Conference Record--1991 IEEE Particle Accelerator Conference*, edited by L. Lizama and J. Chew [IEEE, New York, 1991], vol. 4, pp. 2598-2600.

[6] W.M. Manheimer, S.H. Gold, and Y. Seo, "The Magnicon as a Highly Efficient, High Power, High Frequency Source for Space Power Beaming," in *Proceedings of the Second International Symposium on Power from Space—SPS 91* (Société des Électriciens et des Électroniciens and Société

des Ingénieurs et Scientifiques de France, Paris, France, 1991), pp. 510–514.

[7] V.E. Akimov, Yu.V. Baryshev, B.S. Estrin, M.M. Karliner, I.V. Kazarezov, E.V. Kozyrev, G.I. Kuznetsov, I.G. Makarov, O.A. Nezhevenko, G.N. Ostreiko, B.E. Persov, G.V. Serdobintsev, M.A. Tiunov, V.P. Yakovlev, and I.A. Zapryagaev, "High–Power X–band Pulse Magnicon," in *Proceedings of the Second European Particle Accelerator Conference*, vol. I, pp. 1000–1002, 1990.

[8] O.A. Nezhevenko, I. Kazarezov, E. Kozyrev, G. Kuznetsov, I. Makarov, A. Nikiforov, B. Persov, G. Serdobintsev, M. Tiunov, V. Yakovlev, and I. Zaprygaev, "First Test of the X-Band Pulsed Magnicon," in *Proceedings of the 1993 IEEE Particle Accelerator Conference*, Washington, DC, 1993, in press.

[9] N.C. Jaitly, M. Coleman, S. Eckhouse, A. Ramrus, S.H. Gold, R.B. McCowan, and C.A. Sullivan, "1 MV Long Pulse Generator with Low Ripple and Low Droop," in *Digest of Technical Papers—Eighth IEEE International Pulsed Power Conference*, edited by K. Prestwich and R. White [IEEE, New York, 1991], pp. 161-165.

[10] S.H. Gold, C.A. Sullivan, B. Hafizi, and W.M. Manheimer, "Study of Gain in C-Band Deflection Cavities for a Frequency-Doubling Magnicon Amplifier," *IEEE Trans. Plasma Sci.*, to be published (August 1993).

[11] M.S. Kaschiev, V.A. Kaschieva, I.V. Puzynin, V.V. Gusev, A.I. Fedoseev, I.V. Gonin, and V.V. Paramonov, "Calculation of the Total Oscillation Spectrum in Axisymmetrical RF Cavities and Periodic Structures," in *Proceedings of the IX All-Union Conference on Particle Accelerators*,

Dubna, USSR, INIS-SU-352, CONF-8410203, vol. I, pp. 137-141, 1984 [in Russian].

[12] V.Ya. Ivanov, M.M. Karliner, V.E. Teryayev, and V.P. Yakovlev, "The Method of Boundary Integral Equations for Designing High-Frequency Resonators," *Zh. vychisl. Mat. mat. Fiz.*, vol. 26, no. 12, pp. 1900-1906, 1986; also, *U.S.S.R. Comput. Maths. Math. Phys.*, vol. 26, no. 6, pp. 194-199, 1986.

[13] H.A. Bethe, "Theory of Diffraction by Small Holes," *Phys. Rev.*, vol. 66, pp. 163-182, 1944.

[14] B. Hafizi, S.H. Gold, W.M. Manheimer, and P. Sprangle, "Nonlinear Analysis of a Magnicon Output Cavity," *Phys. Fluids B*, vol. 5, pp. 3045-3055, 1993.

[15] D.G. Myakishev and V.P. Yakovlev, "An Interactive Code SUPERLANS for Evaluation of RF-Cavities and Acceleration Structures," in *Conference Record--1991 IEEE Particle Accelerator Conference*, edited by L. Lizama and J. Chew [IEEE, New York, 1991], vol. 5, pp. 3002-3004.

[16] Yu.V. Baryshev, I.V. Kazarezov, E.B. Kozyrev, G.I. Kuznetsov, I.G. Makarov, O.A. Nezhevenko, B.Z. Persov, M.A. Tiunov, V.P. Yakovlev, and I.A. Zapryagaev, "Electron Optic System for Forming 100 MW Beam with High Current Density and Microsecond Pulse Duration for X-Band Magnicon," in *Proceedings of the VIII International Conference on High Power Particle Beams*, Novosibirsk, vol. I, pp. 598-603, 1990.

[17] See, *e.g.*, J. Benford and J. Swegle, *High-Power Microwaves* (Artech, Boston,1991), pp. 34-35.

[18] B. Hafizi, Y. Seo, S.H. Gold, W.M. Manheimer, and P. Sprangle, "Analysis of the Deflection System for a Magnetic-Field-Immersed Magnicon Amplifier," *IEEE Trans. Plasma Sci.*, vol. 20, pp. 232-239, June 1992.

[19] W. Lawson, J.P. Calame, B.P. Hogan, M. Skopec, C.D. Striffler, and V.L. Granatstein, "Performance Characteristics of a High-Power X-Band Two-Cavity Gyroklystron," *IEEE Trans. Plasma Sci.*, vol. 20, pp. 216-223, 1992.

[20] J.W. Gewartowski and H.A. Watson, *Principles of Electron Tubes* (van Nostrand, New York, 1965), Chap. 9.

TABLE I

MAGNICON DESIGN PARAMETERS

Input:	~1 kW @ 5.7 GHz
Beam:	500 keV, 172 A
Deflection cavities:	3 half-wavelength TM_{110}-mode cavities (1 drive, 2 gain) Cavity Radius~3.2 cm; Cavity Length=2.3 cm; Beam Tunnel Radius=0.5 cm; Beam Tunnel Length=1.9 cm
Penultimate cavity:	π-mode two-section TM_{110} cavity, Cavity Radius~3.2 cm, Cavity Length=5 cm
Output cavity:	TM_{210} mode, Q~800 (for 5.5-mm-diam. beam) Radius~2.15 cm; Length=5 cm
Maximum rf fields at walls: (Penultimate and Output Cavities)	~250 kV/cm
Output:	$f_{out} = 4f_{SLAC} = 11.4$ GHz P ~ 20 MW @ η~24% for 5.5-mm-diam. beam P ~ 50 MW @ η~56% for 2-mm-diam. beam Overall gain ~ 44-48 dB

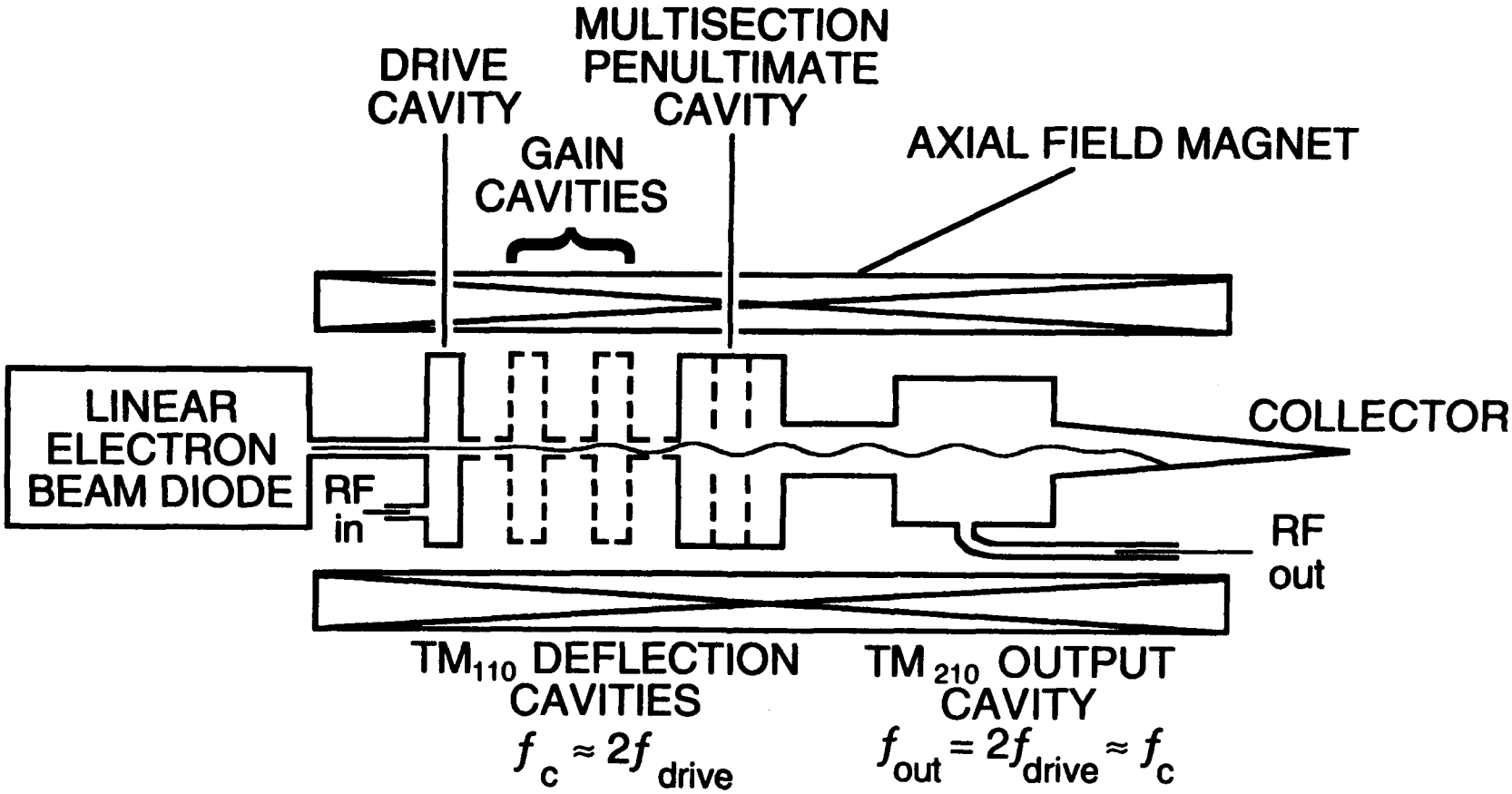

Figure 1. Schematic of frequency-doubling magnicon configuration.

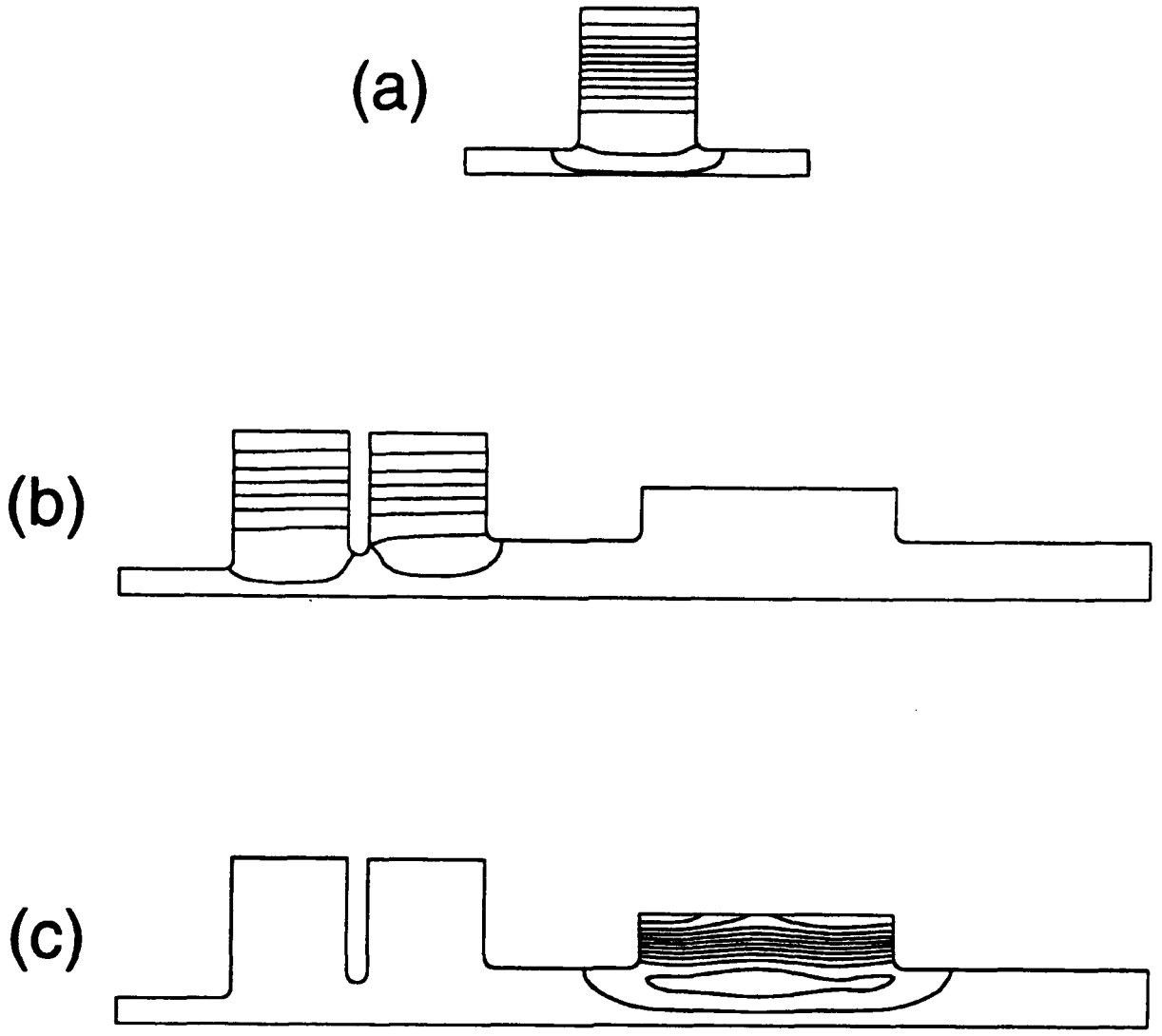

Figure 2. Rf axial electric field lines in (a) the half-wavelength TM_{110} deflection cavities, (b) the two-section TM_{110} π-mode penultimate cavity, and (c) the TM_{210} mode output cavity.

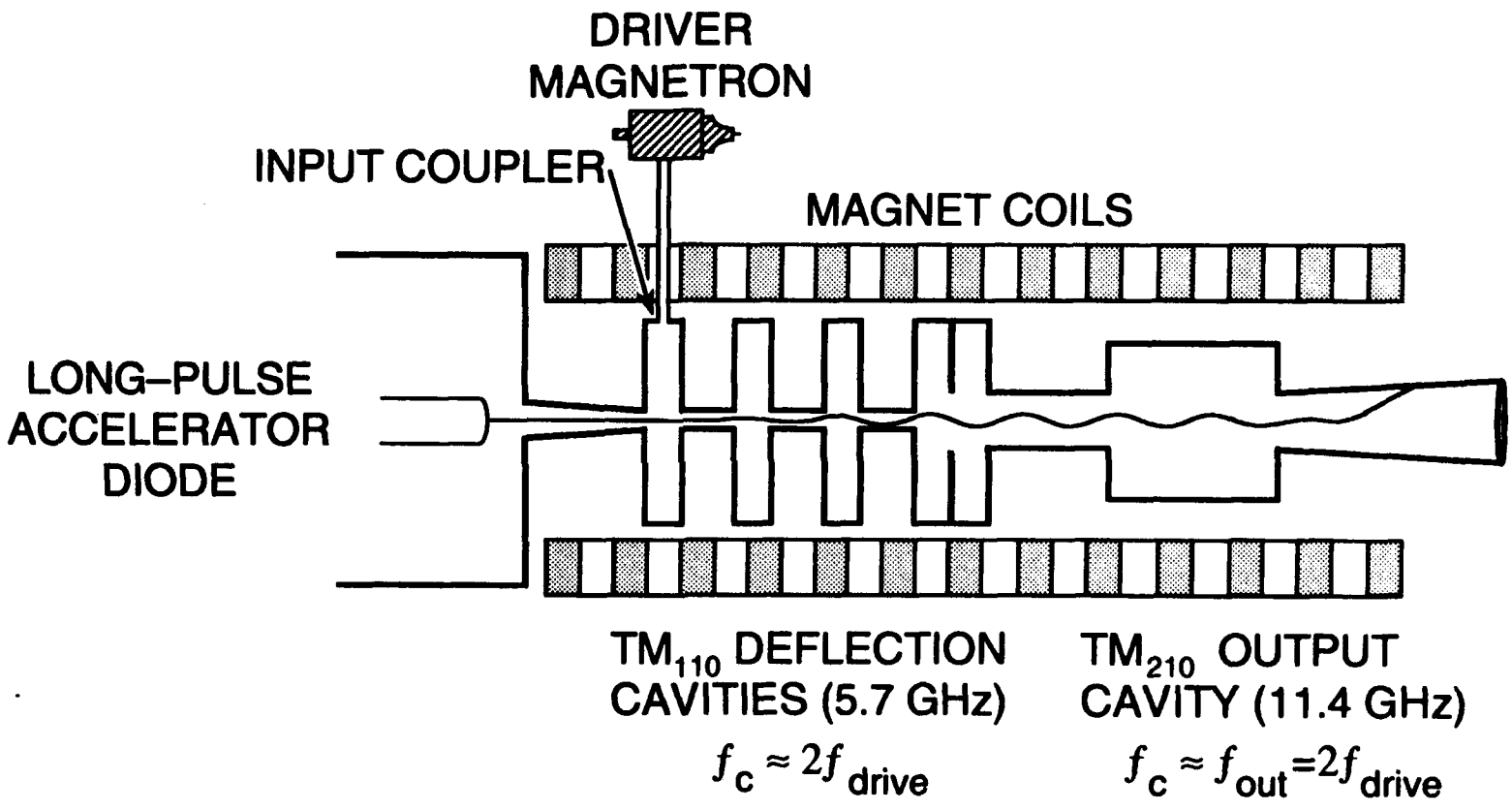

Figure 3. Schematic of the final magnicon design.

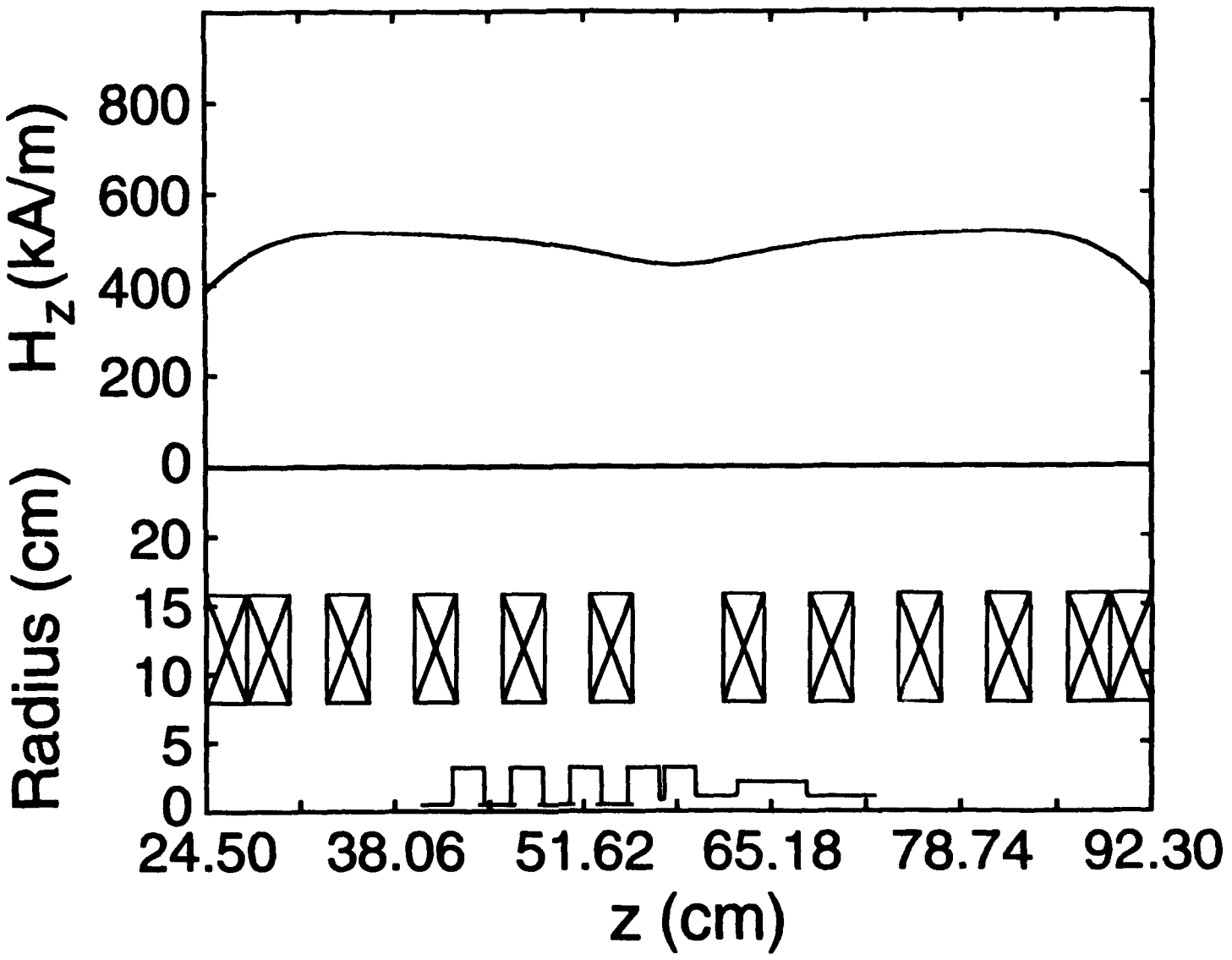

Figure 4. Schematic of the cavities and magnetic field coils, including the axial magnetic field profile used in the simulations.

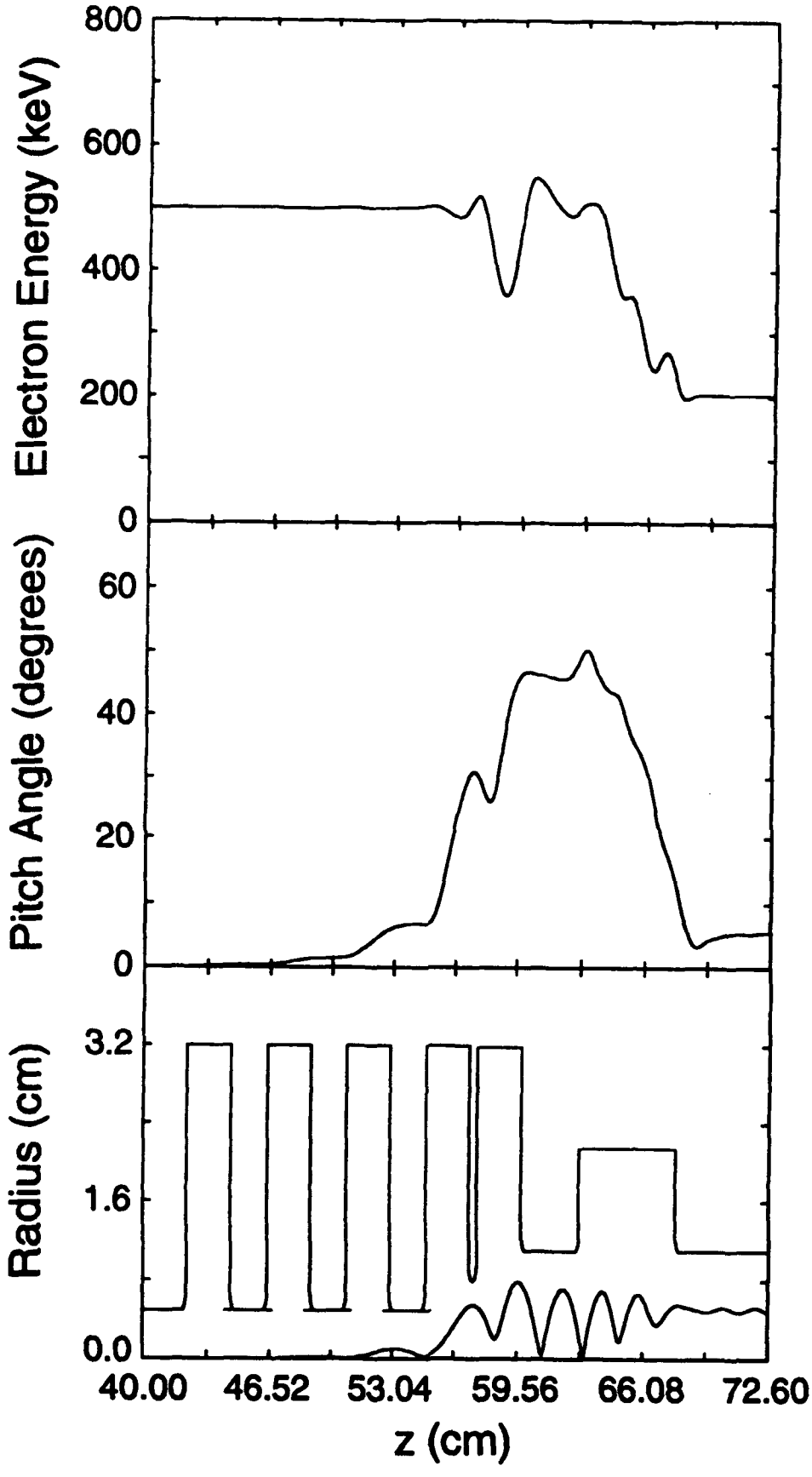

Figure 5. Simulation of the final magnicon design for a single on-axis electron.

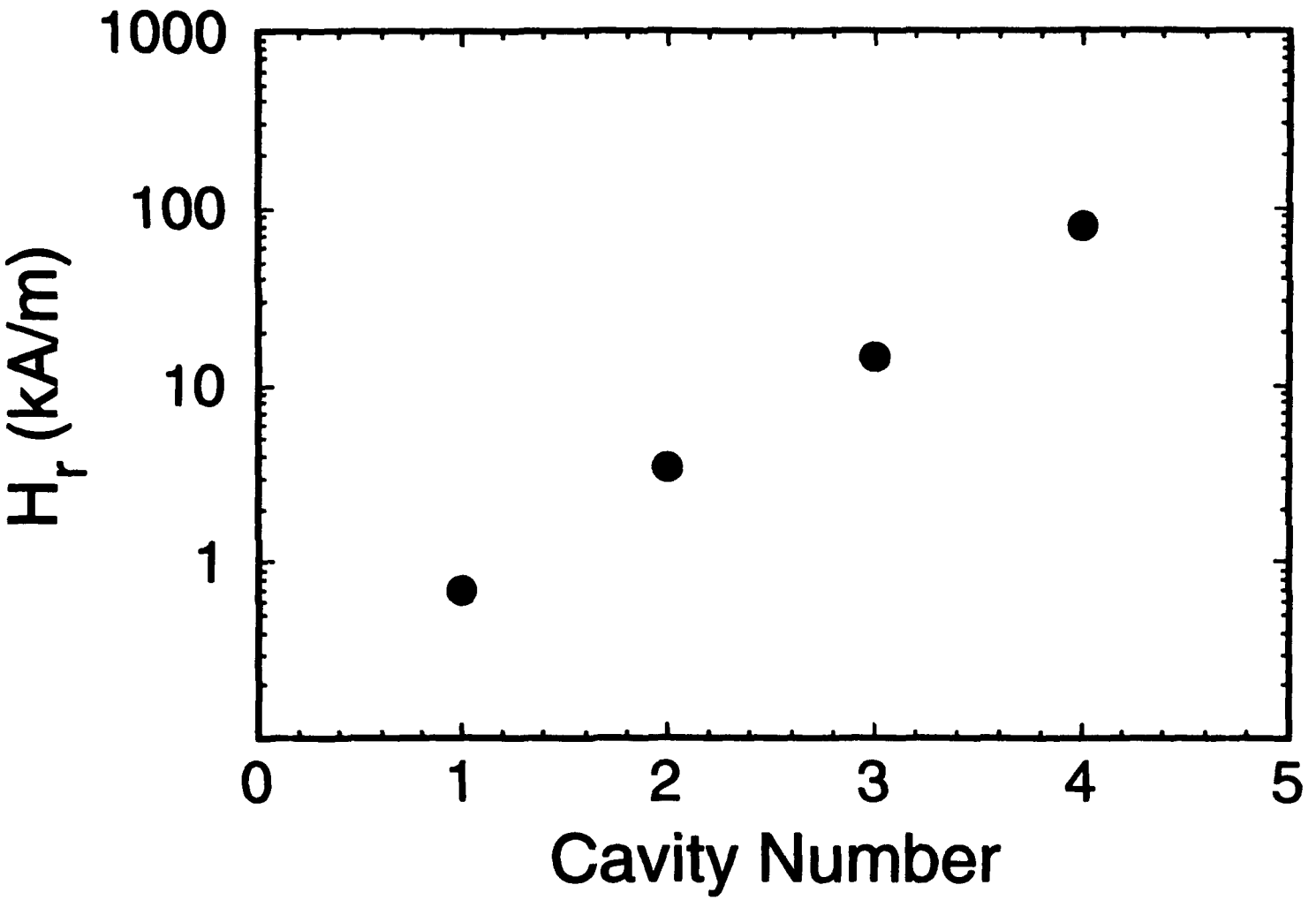

Figure 6. Maximum on-axis value of transverse rf magnetic field versus cavity number, for the final magnicon design.

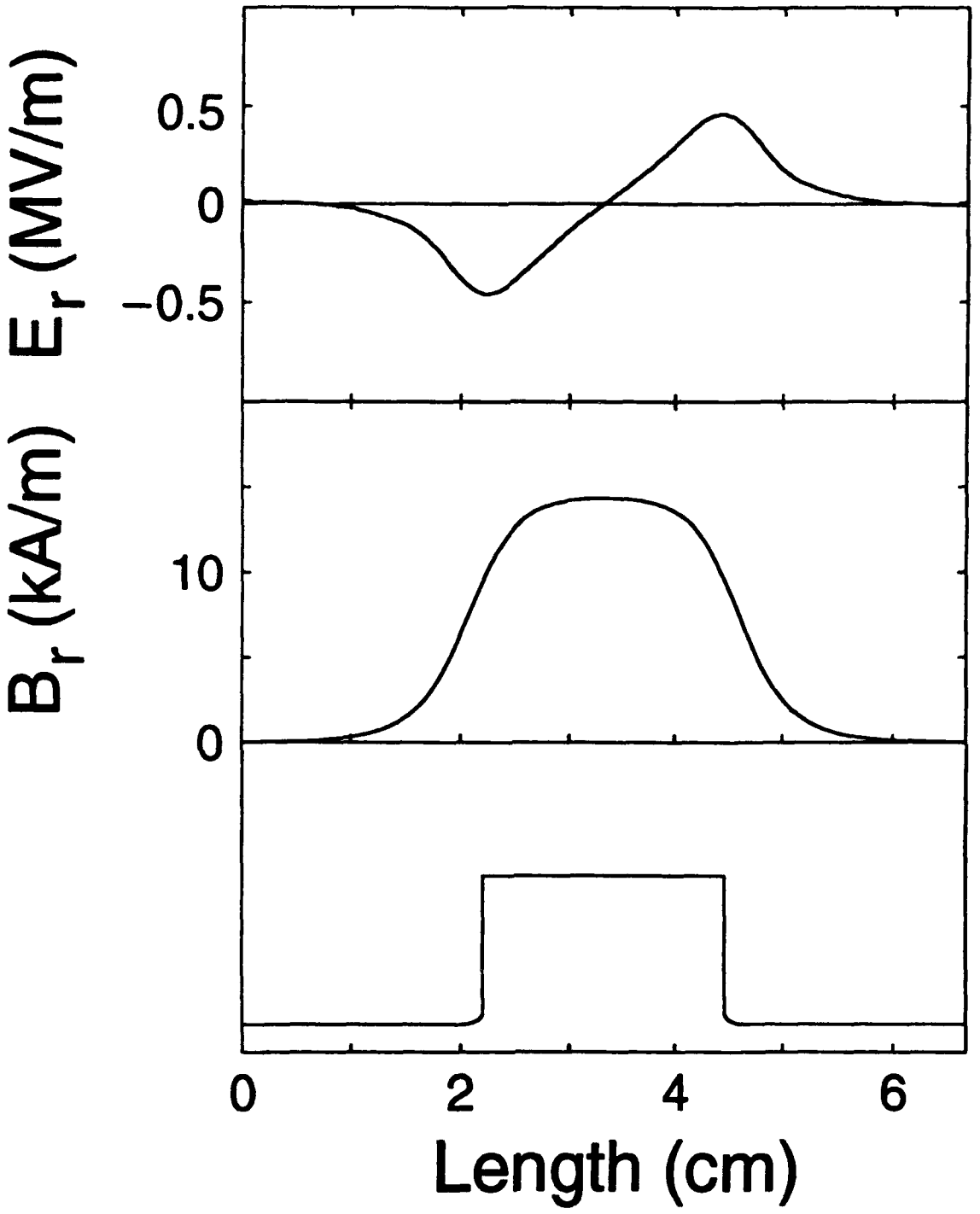

Figure 7. Transverse electric and magnetic fields on the axis of the second gain cavity as a function of position along the axis. The cavity outline is also shown.

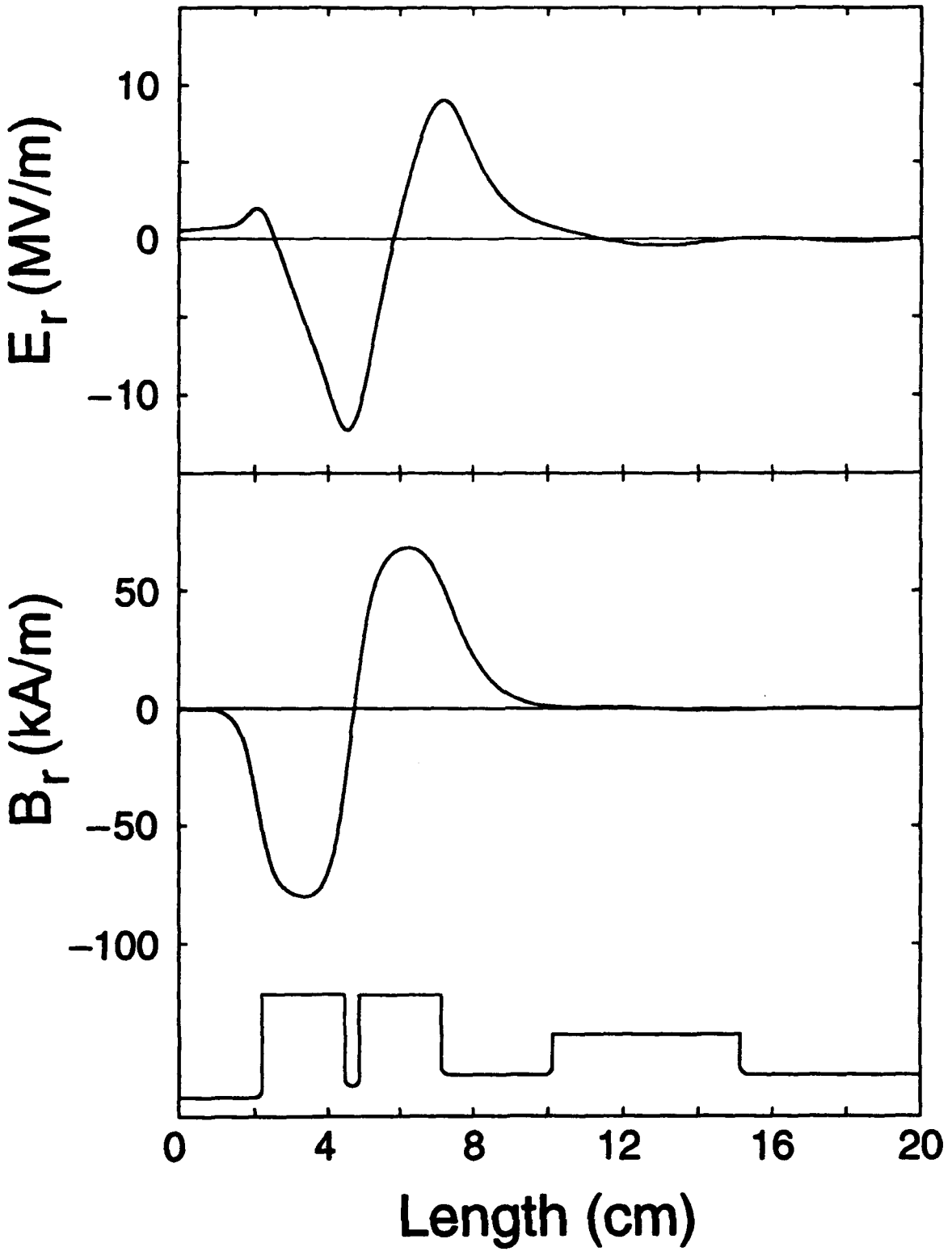

Figure 8. Transverse electric and magnetic fields on the axis of the penultimate cavity mode as a function of position along the axis.

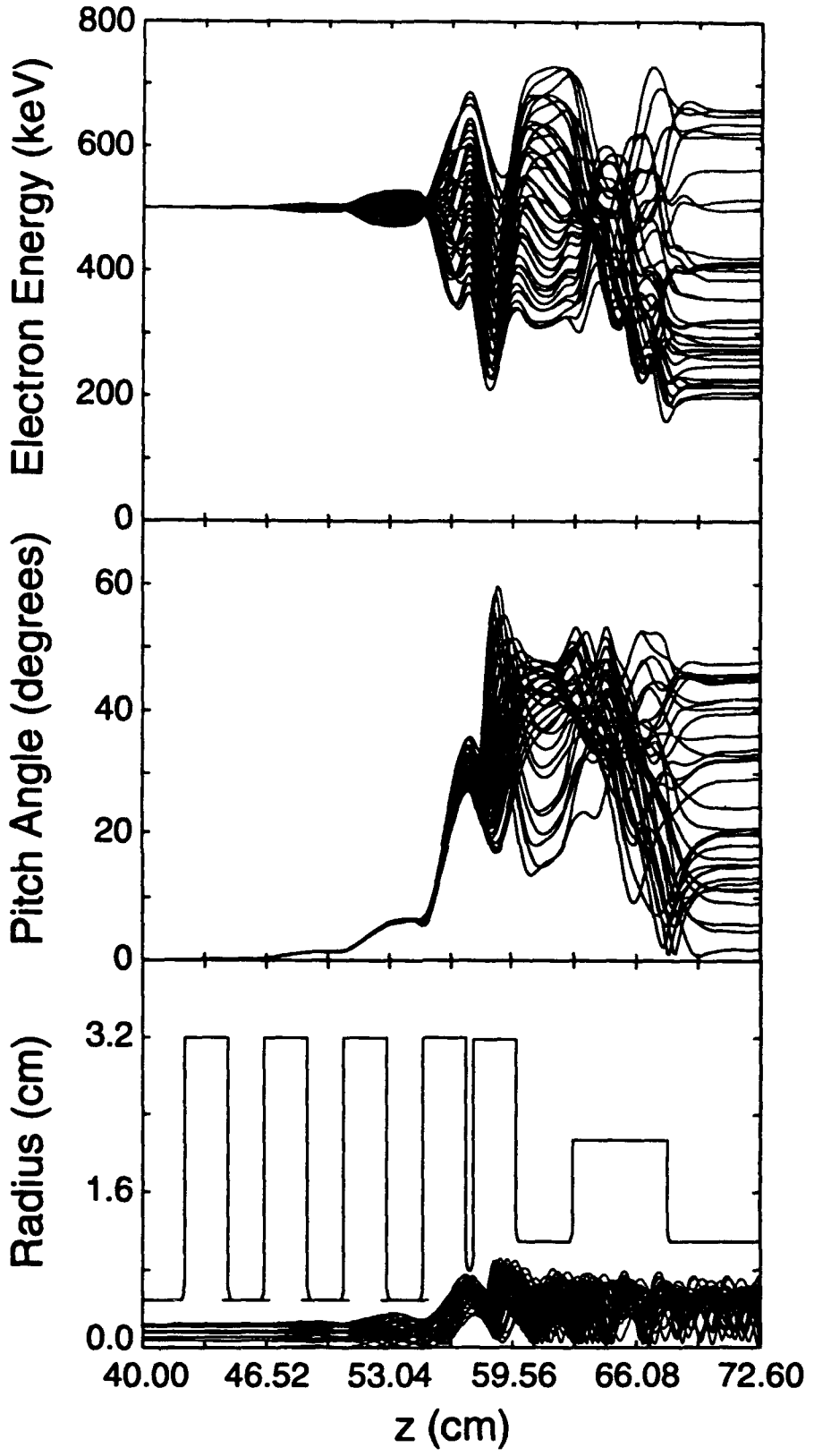

Figure 9. Simulation of the final magnicon design for a 5.5-mm-diameter beam, showing the spatial evolution of electron energy and velocity pitch angle, and the electron trajectory.

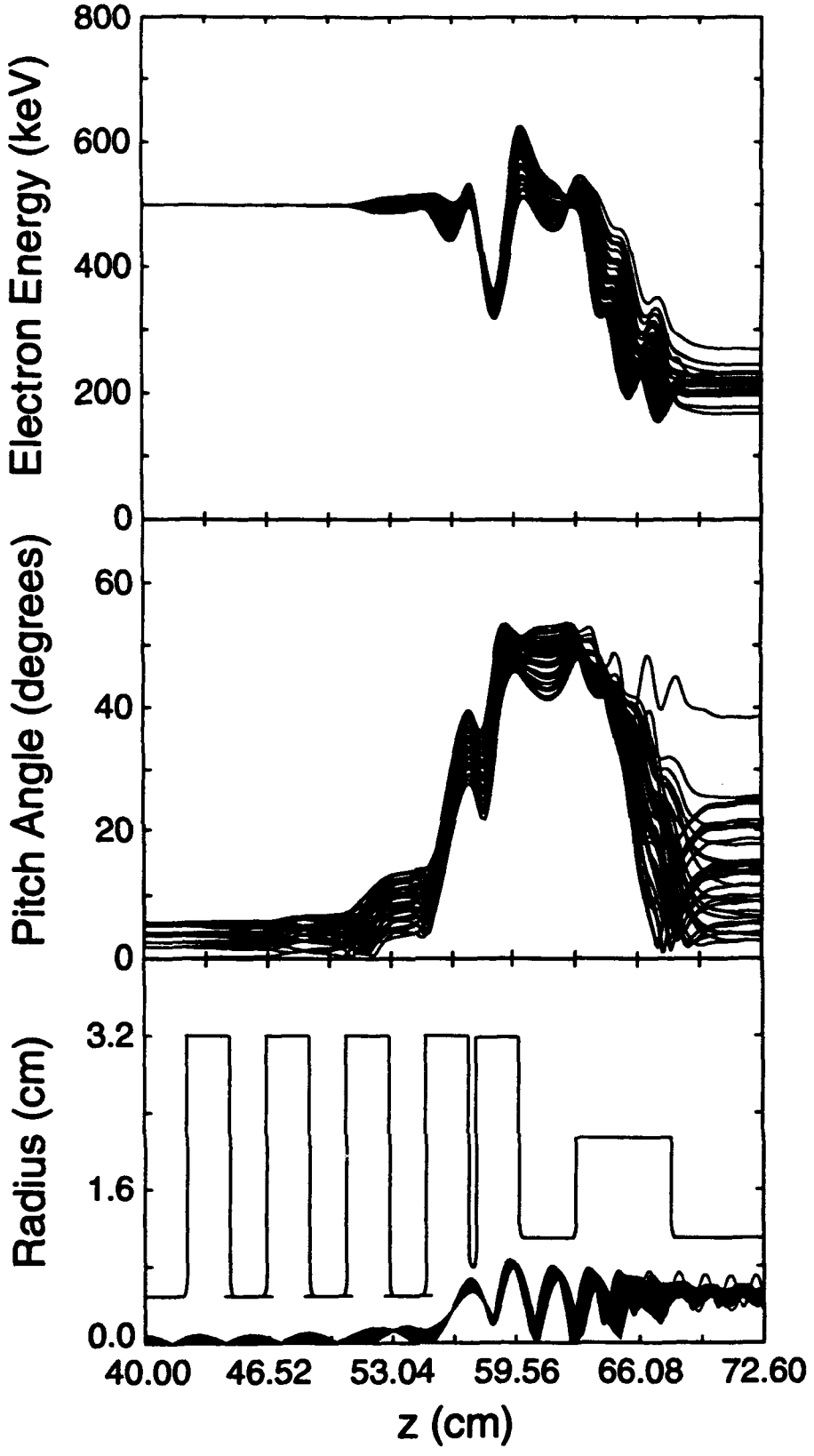

Figure 10. Simulation of the final magnicon design for a 2-mm-diameter beam from a shielded cathode.

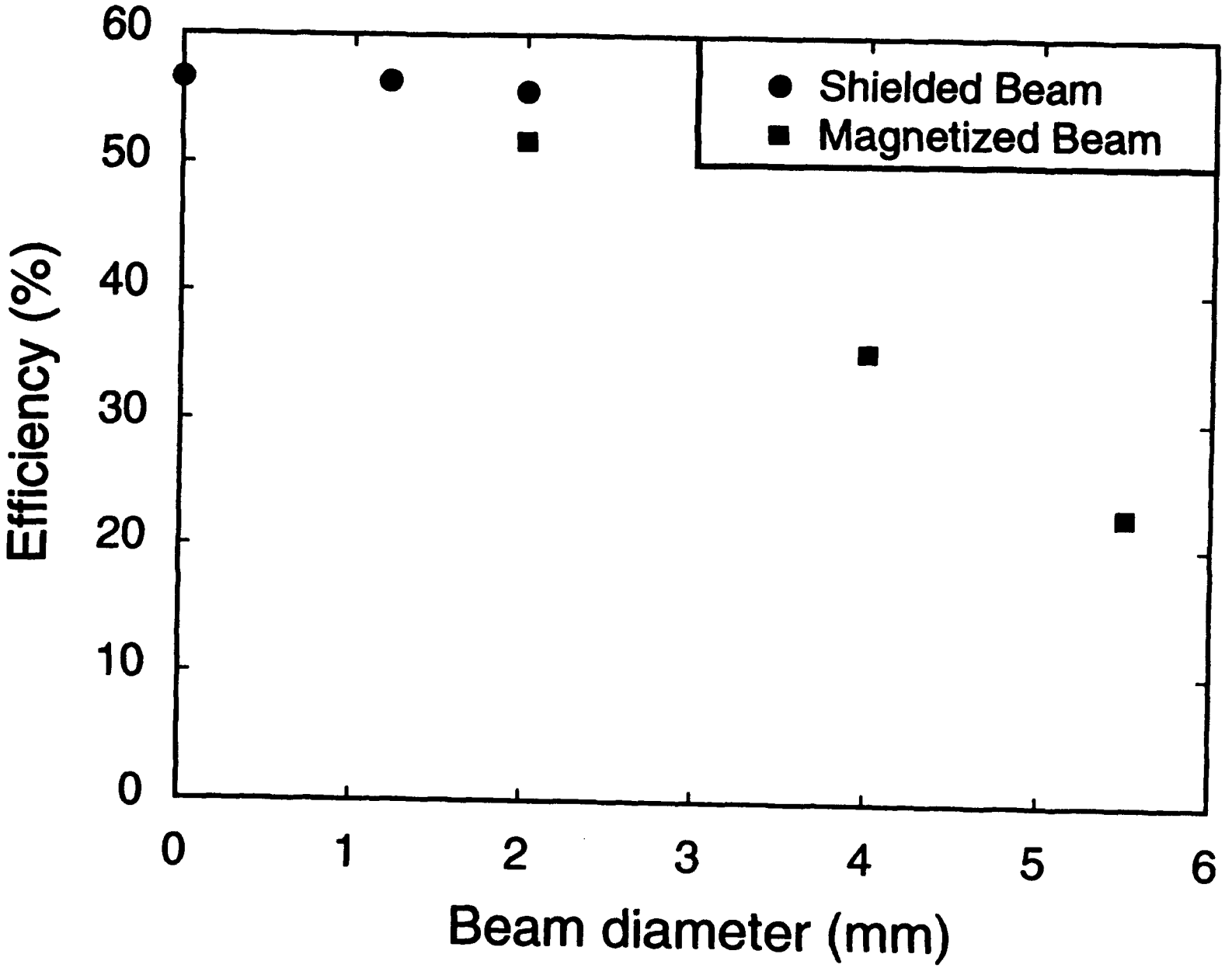

Figure 11. Magnicon efficiency versus beam diameter. Shielded cathode (●) and magnetized beams (■) cases are included. Note that the point at 0 mm is the same for shielded and magnetized beams.

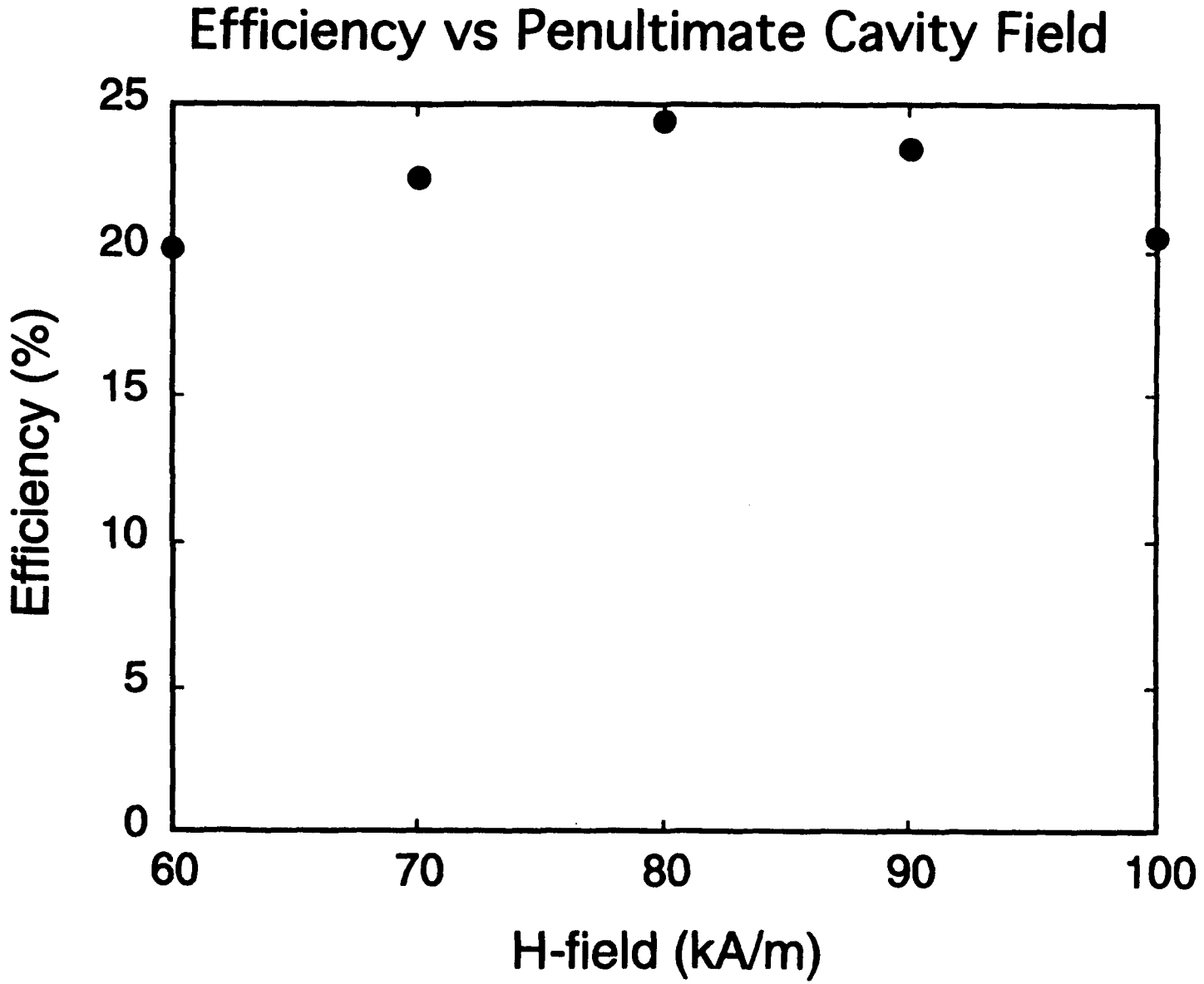

Figure 12. Efficiency of the output cavity versus field in the penultimate cavity.